energies

MDPI

Article

Solidified-Air Energy Storage: Conceptualization and Thermodynamic Analysis

Sandro Hiller [1], Christian Hartmann [1], Babette Hebenstreit [1,2] and Stefan Arzbacher [1,*]

[1] Research Centre Energy, Vorarlberg University of Applied Sciences, 6850 Dornbirn, Austria; sandro.hiller@fhv.at (S.H.); chartmann@gmx.ch (C.H.); babette.hebenstreit@fhv.at (B.H.)
[2] Division of Energy Science, Department of Engineering Sciences and Mathematics, Luleå University of Technology, 971 87 Luleå, Sweden
* Correspondence: stefan.arzbacher@fhv.at

Abstract: Grid-scale electrical energy storage (EES) is a key component in cost-effective transition scenarios to renewable energy sources. The requirement of scalability favors EES approaches such as pumped-storage hydroelectricity (PSH) or compressed-air energy storage (CAES), which utilize the cheap and abundant storage materials water and air, respectively. To overcome the site restriction and low volumetric energy densities attributed to PSH and CAES, liquid-air energy storage (LAES) has been devised; however, it suffers from a rather small round-trip efficiency (RTE) and challenging storage conditions. Aiming to overcome these drawbacks, a novel system for EES is developed using solidified air (i.e., clathrate hydrate of air) as the storable phase of air. A reference plant for solidified-air energy storage (SAES) is conceptualized and modeled thermodynamically using the software CoolProp for water and air as well as empirical data and first-order approximations for the solidified air (SA). The reference plant exhibits a RTE of 52% and a volumetric storage density of 47 kWh per m^3 of SA. While this energy density relates to only one half of that in LAES plants, the modeled RTE of SAES is comparable already. Since improved thermal management and the use of thermodynamic promoters can further increase the RTEs in SAES, the technical potential of SAES is in place already. Yet, for a successful implementation of the concept—in addition to economic aspects—questions regarding the stability of SA must be first clarified and challenges related to the processing of SA resolved.

Keywords: electrical energy storage; thermal energy storage; air energy storage; air clathrate hydrate

check for updates

Citation: Hiller, S.; Hartmann, C.; Hebenstreit, B.; Arzbacher, S. Solidified-Air Energy Storage: Conceptualization and Thermodynamic Analysis. *Energies* **2022**, *15*, 2159. https://doi.org/10.3390/en15062159

Academic Editors: Alon Kuperman and Alessandro Lampasi

Received: 22 February 2022
Accepted: 14 March 2022
Published: 16 March 2022

Publisher's Note: MDPI stays neutral with regard to jurisdictional claims in published maps and institutional affiliations.

Copyright: © 2022 by the authors. Licensee MDPI, Basel, Switzerland. This article is an open access article distributed under the terms and conditions of the Creative Commons Attribution (CC BY) license (https://creativecommons.org/licenses/by/4.0/).

1. Introduction

With the increasing expansion of renewable energy sources for power generation, the integration of their volatile production capacity into the electrical grid infrastructure is becoming an ever greater challenge. To address this challenge, a variety of flexibility measures and electrical energy storage (EES) have been discussed in the literature. See, e.g., the review of Zehrran et al. [1], the discussions about storage demands by Sterner and Stadler [2], as well as recent simulation results from Child et al. [3] and Schill et al. [4]. In general, for low-to-medium (up to 70%) penetration of renewable energy into the electricity supply mix, flexibility measures such as demand-side management and flexible power plants appear most cost effective. However, in a 100% renewable energy system, EES with storage periods of some hours up to a day play a major role.

In this respect, a plethora of solutions for EES have been developed, deployed, or are at the demonstration stage (see the reviews by Chen et al. [5], Gür [6], and Hameer and van Niekerk [7]). All of them aim to meet one or more of the following requirements: high (volumetric) storage density, low storage losses, fast charge and discharge rates, cheap to build, cheap to operate, and cheap to scale. While there are a few solutions that can meet several of these requirements, none of them perform well in all of these aspects. The requirement of scalability is particularly hard to meet, as it demands the

utilization of materials which are both cheap and sufficiently abundant on Earth. Next to an increasing number of materials which are discussed as solutions, particularly for thermo- and electrochemical energy storage systems (see the comprehensive review by Gür [6]), these two criteria are also prominently met by (1) water and (2) air.

(1) Water is predominantly used as an easy-to-transport carrier of potential energy in pumped-storage hydroelectricity (PSH) plants which exhibit superior cost-effectiveness and the highest round-trip efficiency (RTE), between roughly 70% and 80% [8]. As the technology for PSH is now over a hundred years old, mature, and well-tested, PSH provides the largest capacity for grid-scale energy storage to date [8]. However, the expansion of PSH capacity is becoming ever more challenging as the number of sites which are technically and economically feasible for PSH is reducing, as Rehman et al. [8], Kucukali et al. [9], and Lu et al. [10] report independently.

(2) Air, on the other hand, is a ubiquitous gas which serves as the storage medium for internal energy in compressed air energy storage (CAES) systems (see the reviews by Budt et al. [11] and Chen et al. [12]). Excess electricity is used to compress the air and raise its internal energy which can be converted back to electricity by expanding the air in a gas turbine. Due to the low volumetric energy density of CAES (0.5 kWh to 25 kWh per m^3 of compressed air storage [11]), storage is done most cost-effectively underground in large salt caverns. This implies that here, too, suitable geological structures are required for large scale EES, hence limiting the deployment of the technology to a small number of sites, such as the Huntdorf and the McIntosh plant, both described in detail by Budt et al. [11] and Chen et al. [12].

One way to get around the geographic dependence while still benefiting from the advantages of the ubiquity of air is liquid-air energy storage (LAES), a cryogenic energy storage (CES) technology, which has recently been implemented for the first time in a pilot-scale demonstration plant [13]. The idea is to simply liquefy the air and store it in the liquid instead of the compressed state. The 600 volumes of air at standard temperature and pressure (STP) which are contained within one volume of liquid can eventually be used to drive a gas turbine when the liquid is evaporated using low temperature heat. As the liquid air can be readily stored in well-insulated cryogenic containers which minimize the boil-off losses, LAES is free from geological constraints. Moreover, almost all processes and components in an LAES plant are well-known from cryotechnology (e.g., the liquefaction of air), making the design and operation of the plant calculable and low-risk for the operators. Yet, the liquefaction of air is a heat-intensive process which results in only mediocre RTEs of less than about 50%, even when the heat is stored and recycled. This follows from independent thermodynamic analyses of idealized and simplified plants [13–16]. In practice, though, RTEs can also be significantly lower. For instance, Ameel et al. [14] and Borri et al. [17] report RTEs of only 20% and 10%, respectively. This is in part because of the extremely low temperature of the liquid air ($<$77 K) which makes the storage and recovery of cold energy prone to large losses, particularly for extended periods of storage (e.g., many hours to several days).

To overcome the drawbacks of site restrictions and low round-trip efficiencies attributed to CAES and LAES, respectively, this work introduces a novel concept for the large-scale storage of electrical energy using solidified air as the storage medium. Solidified air, i.e., the clathrate hydrate of air, or air hydrate for short (see Koh et al. [18] for a general overview on clathrate hydrates and Miller [19], Pauer et al. [20], and Shoji et al. [21] for details on naturally occurring air hydrate), is an inclusion compound of water and air in which around 170 volumes of air at STP can be stored in one volume of the solid. This makes up a molecular storage tank for compressed air with an achievable air-based volumetric storage density of about one-quarter that of LAES systems. While the utilization of hydrogen-bonded water cavities as the high-pressure containment for air allows for cheap and scalable storage, the disadvantage of a slightly lower storage density could be set off by milder storage conditions. Together this could yield a CES system which alleviates the heat storage-loss problem of LAES but retains and extends its advantages.

Although clathrate hydrates of natural gas, also termed solidified natural gas (SNG) by Linga and coworkers [22–24], are widely discussed as alternative solutions for the storage of chemical energy in the form of natural gas, the usage of air hydrates or solidified air (here used in analogy to SNG) in a CES system has not been considered so far. Based on equilibrium thermodynamics and a well justified assumption, the utilization of solidified air (SA) for EES seems feasible on first thought. Yet, due to the complexity of the phase diagram and a few unknowns with respect to the kinetics and thermodynamics of SA, careful evaluation of the new approach to CES is needed.

Therefore, in this paper, the concept for a SAES system is laid out for the first time, examined, and compared with the state of the art of LAES using a thermodynamic analysis. While the main goal of our analysis is to clarify whether the concept of SAES is technically feasible at all, it is additionally used to provide an initial recommendation as to whether the concept is worth developing further and—if so—where future research must be directed at.

2. Conception

The principle idea behind SAES is to use excess electricity, water, and air, to form SA and store it in heaps or skips on or in ground, respectively. In periods of high electricity demand, the SA is dissociated to recover the water and air, which, similar to LAES, is used to drive a turbine and generate electricity.

The term SA refers to air hydrate [19], an inclusion compound in which the molecules of the air (predominantly N_2 and O_2) occupy cavities formed by a hydrogen-bonded network of water molecules (see Figure 1a for an illustration). The composition of SA is nonstoiciometric, i.e., not all cavities of the structure need to be occupied. However, the maximum occupancy is 5.75 mol of water per mole of air. That relates to approximately 170 volumes of air at STP per volume of hydrate, which is about one-quarter the air storage capacity of liquefied air (600 vol/vol), but relates to approximately 17 MPa, a pressure much larger than that applied in CAES (typically <10 MPa [11,12]).

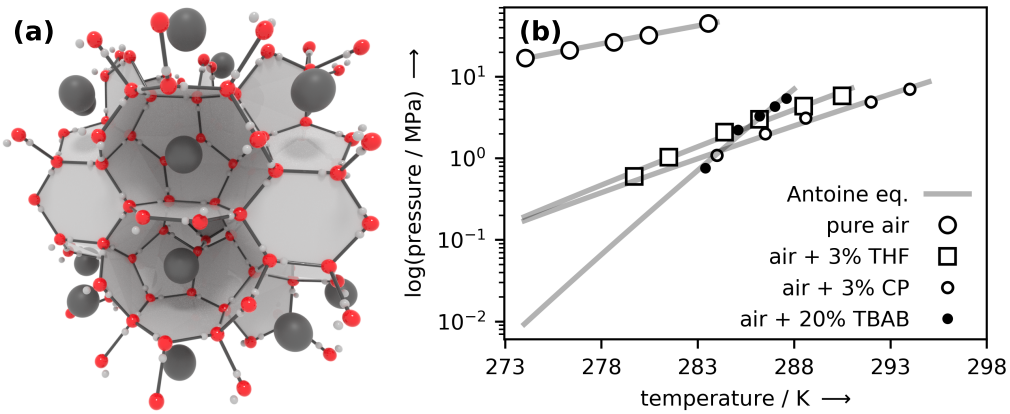

Figure 1. (**a**) Artistic illustration of the molecular structure of SA, i.e., air hydrate. The large grey balls denote air molecules (N_2 and O_2), the red balls denote the oxygen atoms of water molecules which form a hydrogen-bonded network of cavities around the air molecules. (**b**) Hydrate–liquid–vapor equilibrium data for pure air hydrate (data from Mohammadi et al. [25]) and for hydrates of air with the growth-promoting substances Tetrahydrofuran (THF), Cyclopentane (CP), Tetrabutylammonium bromide (TBAB) (data from Yang et al. [26]). The solid grey lines fit the data and denote the phase boundary above which the hydrate is thermodynamically stable (also see Lipenkov and Istomin [27] and Mohammadi and Richon [28] for a discussion of the phase diagram).

Due to its water-rich composition, many of the SA's properties, such as its appearance or density (approx. 1 g/cm^3 [29]), resemble those of ice. Likewise, the heat of their dissociation is comparable to the heat of fusion of ice (334 kJ/kg [30]). While due to their large heat of fusion, both ice and gas hydrates can be utilized for thermal energy storage (see the reviews by Saito [31] for ice and Wang et al. [32] for gas hydrate thermal energy

storage), gas hydrates can additionally be used to store electrical energy if their ability to act as molecular storage vessel for gases is exploited. SA can be formed by bringing together liquid water and air at conditions above the hydrate–liquid–vapor equilibrium curve (the solid gray lines in Figure 1b), which means at moderately low temperatures but high pressures. It can be dissociated by exposing it to conditions below that curve, that is, by superheating or underpressurizing with respect to stability conditions. The equilibrium curve and its variation with temperature is very important in the context of this paper, because, by varying the temperature, the SA formation and dissociation pressure can be modified drastically. For instance, one could form SA at low temperature/pressure and dissociate it at higher temperature/pressure to minimize the work of compression while maximizing that of turbine expansion. Furthermore, as shown in Figure 1b, the addition of small amounts of stability-promoting substances such as THF, CP, and TBAB, can have a dramatic effect on the equilibrium curve and thus on both formation and dissociation conditions [26]. Although promoters and their effects must be addressed because of their potential to improve the RTE of a future SAES plant, for ease of understanding, stability-promoting substances are left out in our analysis of a very first reference case.

A key aspect of our concept for SAES is the storage of the synthesized SA at the most cost-efficient conditions, i.e., preferably at ambient conditions. Yet, as can be seen from the phase diagram in Figure 1b, SA is far from thermodynamic stability at ambient conditions. Therefore, storage in the stable form is unsuitable for our purposes. However, a kinetic anomaly termed "self-preservation" (SP) [33], which results in very low rates of dissociation at conditions far outside the stability region, is likely to allow for a medium-term (days to weeks) storage of SA at ambient pressure and temperatures just below 273 K with minute amounts of "boil-off" losses. While SP has been reported numerous times for hydrates of CH_4 [34,35] and CO_2 [36,37], little is known for hydrates of air, probably because it seemed not relevant enough to this date. However, several reports [38–40] of SP for O_2 and N_2—the major constituents of air—render the occurrence of SP in SA plausible. In case SP in SA is similarly effective as in hydrates of CH_4, SA could be stored at subzero temperatures and ambient pressure for months with losses of only a few percent [41]. Additionally, due to the strongly endothermic transition, every dissociation of SA cools down the environment. Therefore, when the stored SA is thermally well insulated, it does not have to be actively cooled.

For the rest of this work we build on the assumption of pronounced SP with the full knowledge that its refutation will render the whole concept purely theoretical. Even then, though, this work can still be regarded a long-missing potential application needed to stimulate research on SP in hydrates of air.

3. Materials and Methods

In this section, a theoretical process for SAES is outlined before a thermodynamic model for the steady-state operation of a reference plant is developed. Besides, performance parameters are defined to allow for comparisons with competing EES technologies.

3.1. Plant Description

The SAES plant is conceptualized in the process scheme in Figure 2.

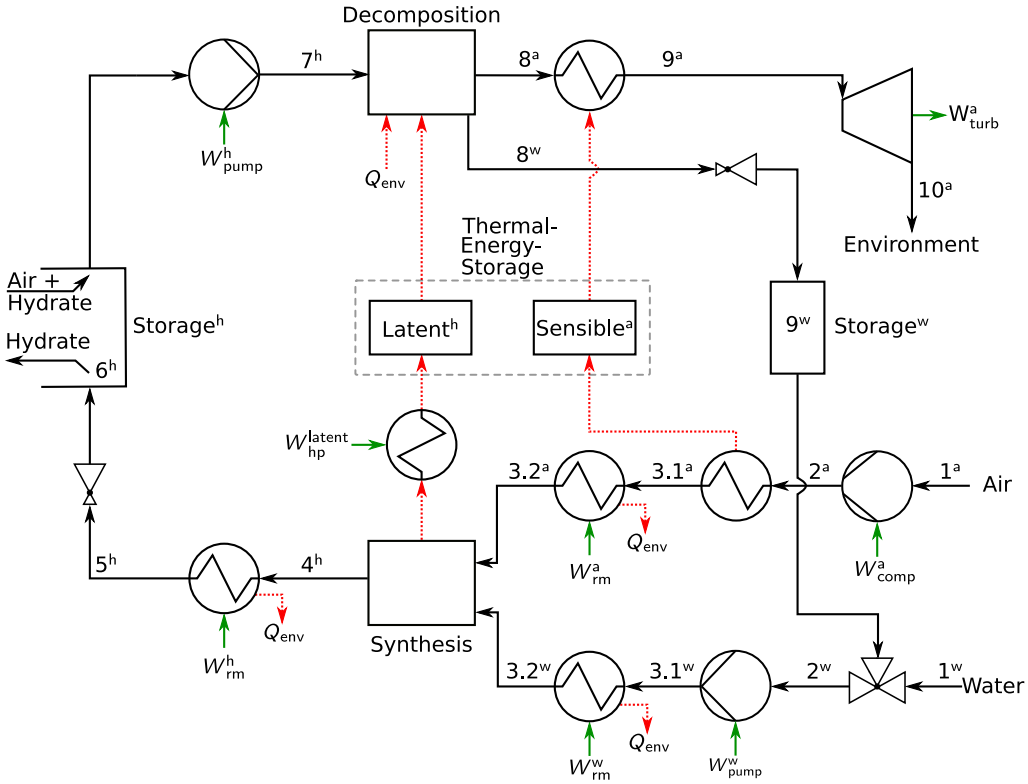

Figure 2. Simplified process scheme of a reference plant for SAES. Solid black lines denote pathways for media transport. Dashed red lines are used to indicate heat transport. Short green arrows are used to label energy flows. In the state labeling, consecutive numbers are used according to a "energy charging → energy storage → energy discharging" order. Superscripts "a", "w", and "h" denote air, water and hydrate (i.e., SA), respectively.

Similar to CAES and LAES, electrical energy is used to compress air (1^a to 2^a). However, instead of storing the pressurized air directly, like in CAES, or liquefying the air, as in LAES, SA is formed from the pressurized air and water (3 to 4). Before entering the reactor, air and water are brought to formation conditions (1 to 3.2). After its formation in the reactor, the SA is extracted and pelletized (as described by, e.g., Rehder et al. [42]) for ease of transport. Note that this step is neither shown in the process scheme nor taken into account in the calculation. Other options for SA processing, such as in a slurry or via "dry water" [43], complicate the process scheme and are therefore not considered for now. The pelletized SA is cooled below 0 °C and the pressure is released (4^h to 6^h). At this state, i.e., at ambient pressure and moderately below 0 °C, the SA reaches SP conditions and can be stored in the SA storage. During discharge, the process is reversed. To this end, the SA is first pressurized by a high-density solids pump, e.g., a single or two-cylinder piston pump (6 to 7). The dissociation of the SA to air and water takes place in the dissociation reactor (7 to 8). Eventually, the air is heated (8^a to 9^a) and expanded in a turbine (9^a to 10^a) to recover electricity.

Both processes, the compression/expansion of air, as well as the formation/dissociation of SA, are heat intensive. Therefore, three thermal energy storage (TES) units are integrated: a sensible heat storage, which is charged by the hot air after the compressor (2^a to 3.1^a) and discharged by the cool air before the turbine (8^a to 9^a); a latent heat storage, which is charged during the exothermic SA formation (3 to 4) and discharged during the endothermic SA dissociation (7 to 8); and a water tank, to reuse the cold water exiting the dissociation reactor (8^w) in the next cycle. Water losses are compensated by mixing with water at ambient conditions (1^w to 2^w). Where no heat integration is possible, refrigeration machines and heat pumps are used. To account for minimum temperature difference constraints as well as heat losses in the storage units, two refrigeration machines are

integrated for air and water, to ensure the attainability of the formation conditions (3.1 to 3.2). Another refrigeration machine is used to cool the SA after formation (4 to 5) to the storage temperature. A heat pump, integrated between the formation reactor and the latent heat storage unit, is operated only in case the minimum temperature difference constraint cannot be met for charging the latent heat storage unit. During discharge, no further refrigeration machines or heat pumps are used. When the heat stored in the latent heat storage unit is not sufficient to completely dissociate the SA, low-temperature ambient heat can be used in addition. The sensible heat storage unit enables the reuse of the heat of compression and determines the inlet temperature at the turbine.

In this very first analysis of SAES, one-stage compression and expansion are assumed for the air. This leads to unrealistically high temperatures and compression rates. It is believed, though, that this approach still allows for valuable insights into the SAES concept. Clearly, upon further developing the idea, multistep compression and expansion have to be considered.

3.2. Plant Modeling

A few simplifications had to be made in the thermodynamic modeling of the SA due to lack of better data. While there are thermodynamic models and simulations available for the prediction of the hydrate–liquid–vapor curve (see the compilation by Khan et al. [44]), accurate predictions of enthalpy changes due to combinations of both phase transition and change of state are still missing. Therefore, the specific enthalpy change Δh_{tr} of phase transition (formation and dissociation) is modeled using the available data of the hydrate–liquid–vapor equilibrium (cf. Figure 1) and the Clapeyron equation

$$\Delta h_{\mathrm{tr}} = T \Delta v (\mathrm{d}p/\mathrm{d}T). \tag{1}$$

The exact procedure is described in great detail by Anderson [45,46]. The change of enthalpy caused by a change of state without phase transition can be described by

$$\mathrm{d}h = \left(\frac{\partial h}{\partial T}\right)_p \mathrm{d}T + \left(\frac{\partial h}{\partial p}\right)_T \mathrm{d}p = c_p \,\mathrm{d}T + \left[v - T\left(\frac{\partial v}{\partial T}\right)_p\right] \mathrm{d}p. \tag{2}$$

Both the variation of c_p [29] as well as the thermal expansivity [47] are small over the range of temperatures considered. Further, SA is nearly incompressible [48]. Consequently, Equation (2) simplifies to

$$\mathrm{d}h \approx c_p \,\mathrm{d}T + v \,\mathrm{d}p, \tag{3}$$

where both $c_p = 2.1$ kJ/kg/K [29] and $v = 1.07$ cm^3/g [49] are assumed to be constant for all conditions considered.

The modeling of air and water does not require such simplifications and is done using the Python wrapper to the software CoolProp [50], an open-source database for fluid and humid air properties. The discrepancy between the simplifications necessary in the modeling of SA and the accurate modeling of water and air naturally results in uncertainties with respect to both the thermodynamic states and the energy balances. In view of other unknowns of much larger magnitude (e.g., the degree of SP, losses due to technical challenges in the handling of SA, etc.) these can be neglected, though.

The modeling of the plant components is done using enthalpy balances according to the parameters listed in Table 1.

Except for the storage units, heat losses are generally neglected. Compressors, pumps, and turbines are described via the isentropic efficiencies η_{comp}, η_{pump}, and η_{turb}, respectively. For ease of comparison, the isentropic efficiencies are chosen in agreement with those used for the modeling of an LAES plant [13]. The expansion valve is assumed to be isenthalpic. The refrigeration machines and heat pumps are calculated with fixed coefficients of performance β_{rm} and β_{hp}, respectively. Heat exchangers are modeled isobarically with fixed minimum temperature differences $\Delta T_{\mathrm{sensible}}$ and $\Delta T_{\mathrm{latent}}$ for the sensible and the

latent heat transfer, respectively. The heat losses of the sensible and the latent heat storage are modeled using the storage efficiencies η_{sensible} and η_{latent}. h_{latent} and c_{sensible} denote the specific phase change enthalpy for the latent heat storage and the specific heat capacity for the sensible heat storage, respectively. The storage efficiencies and volumetric capacities are loosely calibrated to gravel beds for the sensible heat storage and to paraffin for the latent heat storage (see ref. [2] for typical values). In general, a pronounced degree of SP for the storage of SA is assumed, but some "boil-off" losses due to an intake of heat cannot be avoided. These losses are modeled by the hydrate storage efficiency η_{hs}. The hydration number efficiency η_{hn} allows deviations from the stoichiometric hydration number to be accounted for and reduces the air storage capacity of the SA. The void fraction η_{vs} is used to model the fraction of air-filled void space in the SA pellet with respect to its volume.

Table 1. Plant parameters of reference case.

Parameter	Value	Parameter	Value	Parameter	Value
T_{env}	298 K	T_{form}	278 K	T_{diss}	274 K
T_{storage}	273 K	$\Delta T_{\text{sensible}}$	20 K	ΔT_{latent}	2 K
p_{env}	0.1 MPa	p_{form}	25.3 MPa	p_{diss}	16.6 MPa
p_{storage}	0.1 MPa				
η_{comp}	0.85	η_{pump}	0.90	η_{turb}	0.85
η_{hs}	0.975	η_{hn}	1.0	η_{vs}	0.2
η_{sensible}	0.80	η_{latent}	0.95	$\beta_{\text{rm}}^{\text{a}}$	7
$\beta_{\text{rm}}^{\text{w}}$	6	$\beta_{\text{rm}}^{\text{h}}$	6	$\beta_{\text{hp}}^{\text{latent}}$	8
h_{latent}	154 MJ m^{-3}	c_{sensible}	1.5 MJ m^{-3} K^{-1}		

In the simulations of SAES plant operation, all parameters listed in Table 1 can be selected within physically acceptable ranges, while all other states are derived from the enthalpy balances as described above. Typically, efficiencies are fixed before the start of the simulation and the input parameters environment temperature T_{env}, formation temperature T_{form}, dissociation temperature T_{diss}, and SA storage temperature T_{storage} are varied to find optimal conditions of operation.

3.3. Key Indicators

One of the most important indicators of an energy-storage system is the RTE. For the SAES system, the RTE is calculated by

$$\eta_{\text{rt}} = \frac{W_{\text{out}}}{W_{\text{in}}} = \frac{W_{\text{turb}}^{\text{a}} - W_{\text{pump}}^{\text{h}}}{W_{\text{comp}}^{\text{a}} + W_{\text{pump}}^{\text{w}} + W_{\text{rm}}^{\text{a}} + W_{\text{rm}}^{\text{w}} + W_{\text{rm}}^{\text{h}} + W_{\text{hp}}^{\text{latent}}}. \tag{4}$$

This relates the net electricity W_{out}, obtained upon discharging, to the electricity that had to be used for charging.

Another important parameter for characterizing stationary EES systems is the volumetric energy density which expresses the amount of energy stored per unit volume. Considering only the air stored in the SA, the volumetric (solidified) air-based energy density is given by

$$w_{\text{v}}^{\text{a}} = \frac{W_{\text{out}}}{V_{\text{storage}^{\text{h}}}}. \tag{5}$$

To account for the size of the TES system, which is a crucial part of any energy-storage system in which a gas is compressed and expanded, the total energy density

$$w_{\text{v}}^{\text{tot}} = \frac{W_{\text{out}}}{V_{\text{storage}^{\text{h}}} + V_{\text{sensible}^{\text{a}}} + V_{\text{latent}^{\text{h}}} + V_{\text{storage}^{\text{w}}}} \tag{6}$$

is defined in addition.

4. Results and Discussion

This section provides a thermodynamic analysis of the SAES reference plant, followed by the determination of optimal operating conditions and a sensitivity analysis.

4.1. Thermodynamic Analysis

The SAES plant outlined above is modeled using the reference parameters provided in Table 1. As the following analysis will show, these parameters optimize the RTE of the reference plant. An overview of the corresponding states of air, water, and SA is provided in Table 2 for all components of the plant. Key indicators are summarized and compared to a LAES plant in Table 3.

While the RTEs are fairly similar, there is a significant difference in the energy densities. That is mainly because of the more than three-fold density of air in the liquid state compared to SA. The total energy density of LAES including TES has not yet been reported, though, a similar reduction with respect to the air-based value seems reasonable. The big difference between $w_{\mathrm{v}}^{\mathrm{a}}$ and $w_{\mathrm{v}}^{\mathrm{tot}}$ already indicates the importance of TES in the SAES plant. This is highlighted even more by the following figures: To generate a net electricity W_{out} of 1.000 kWh, roughly 1.754 kWh and 2.205 kWh of heat have to be stored in the sensible and latent heat storage unit, respectively. For comparison, the compressor ($W_{\mathrm{comp}}^{\mathrm{a}}$) and turbine work ($W_{\mathrm{turb}}^{\mathrm{a}}$) are 1.729 kWh and 1.107 kWh , respectively.

Table 2. States for the reference case.

State	1	2	3.1	3.2	4	5	6	7	8	9	10
T^{a}/K	298	1474	314	278	-	-	-	-	274	1243	468
p^{a}/MPa	0.1	25.3	25.3	25.3	-	-	-	-	16.6	16.6	0.1
T^{w}/K	298	278	278	278	-	-	-	-	274	278	278
p^{w}/MPa	0.1	0.1	25.3	25.3	-	-	-	-	16.6	0.1	0.1
T^{h}/K	-	-	-	-	278	261	273	273	-	-	-
p^{h}/MPa	-	-	-	-	25.3	25.3	0.1	16.6	-	-	-

Table 3. Key indicators for the reference case of SAES and for LAES.

Indicator	SAES	LAES [15]
Round trip efficiency η_{rt}	52 %	54 %
Energy density $w_{\mathrm{m}}^{\mathrm{h}}$	0.047 kWh kg^{-1}	0.12 kWh kg^{-1}
Air-based energy density $w_{\mathrm{v}}^{\mathrm{a}}$	47 kWh m^{-3}	104 kWh m^{-3}
Total energy density $w_{\mathrm{v}}^{\mathrm{tot}}$	19 kWh m^{-3}	-

To better illustrate these relations, Figure 3 shows a detailed analysis of the works during charging and discharging, again normalized to a net work output of 1.000 kWh.

While $W_{\mathrm{comp}}^{\mathrm{a}}$ and $W_{\mathrm{turb}}^{\mathrm{a}}$ dominate the picture, the works necessary for the compression of water ($W_{\mathrm{pump}}^{\mathrm{w}}$) and SA ($W_{\mathrm{pump}}^{\mathrm{h}}$) stand out as well. As together they sum up to about 25% of the net work output, potential improvements of the RTE are possible by either storing at high pressures instead of the two expansions in the system or by using a water turbine in the expansion process. The arrow in the storage stage termed "different losses" is used to close the enthalpy balance. It combines all heat and storage losses, but also all other losses associated with the various processes executed during charging.

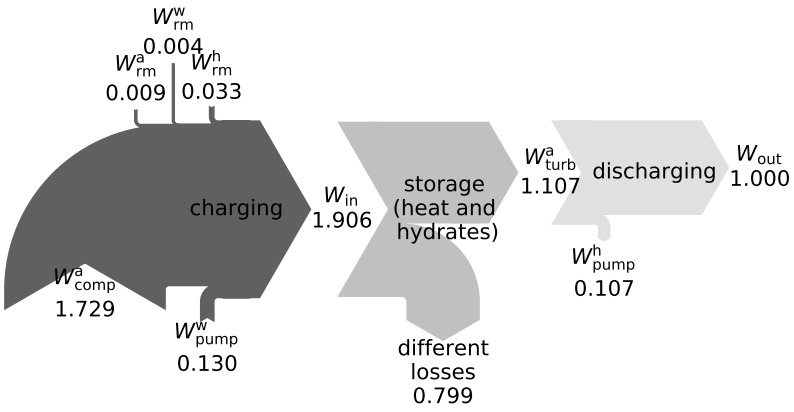

Figure 3. Sankey diagram to illustrate the relation between works (normalized to W_{out}) occurring in the SAES reference case.

4.2. Optimum Operating Conditions

A further analysis of the SAES plant aims at exploring the RTE of the plant while varying the main operational parameters. Figure 4a displays the RTE at different formation and dissociation temperatures.

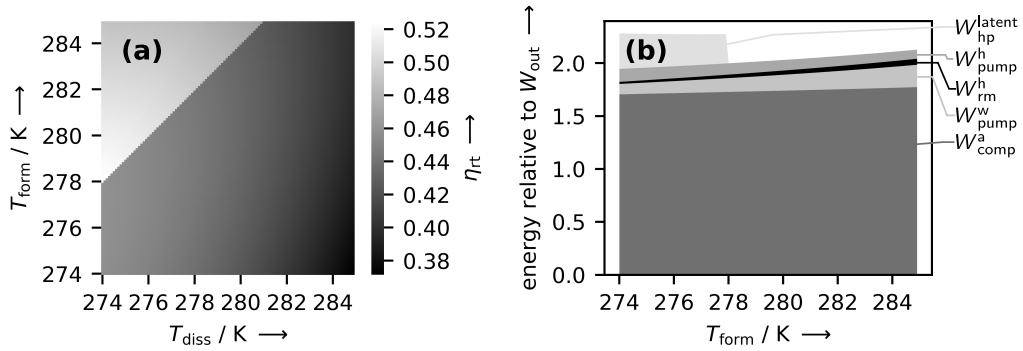

Figure 4. (**a**) Heat map of the RTE as a function of the formation and dissociation temperature. Bright spots indicate a high efficiency, dark spots a low efficiency. (**b**) Sum of process works, normalized to a net work output of 1.000 kWh, as a function of formation temperature. The dissociation temperature is kept constant at 274 K. Note that W^{a}_{rm} and W^{w}_{rm} are negligible on the scale of the graph and omitted for better readability.

The highest RTE is attained at the lowest possible dissociation temperature of 274 K and a formation temperature of 278 K, i.e., conditions also used in the reference case. This indicates that lower formation/dissociation temperatures and thus lower pressures are, in general, favorable. The sudden increase in RTE along a diagonal step can be explained with the help of Figure 4b. Therein, all energies to be expended are displayed as a function of formation temperature while the dissociation temperature is kept constant at 274 K. This can be interpreted as a line plot from the leftmost lower corner in Figure 4a to the top. Following this line, the RTE jumps abruptly as soon as a formation temperature of 278 K is reached. This is because at 278 K the latent heat pump (W^{latent}_{hp}) is no longer needed to ensure heat flow from the formation to the dissociation reactor. Consequently, the expended energy drops and the RTE increases. According to this observation, the dissociation pressure is best kept below the formation pressure to obtain high RTE. This is in contrast to the naive idea to use higher pressures at the turbine inlet than at the compressor outlet to both decrease compressor work and increase turbine work for maximal efficiency, an idea that the authors of this paper also initially fell for. According to the phase diagram in Figure 1, this would imply a higher dissociation than formation temperature. When a latent heat pump is to be

avoided for enhanced efficiency, this is only possible with an external heat supply for the dissociation, an option not further followed in this paper.

4.3. Sensitivity Analysis

In addition to the effect of different temperatures, the sensitivity of the RTE to heat storage and other parameters is investigated in Figure 5a,b, respectively.

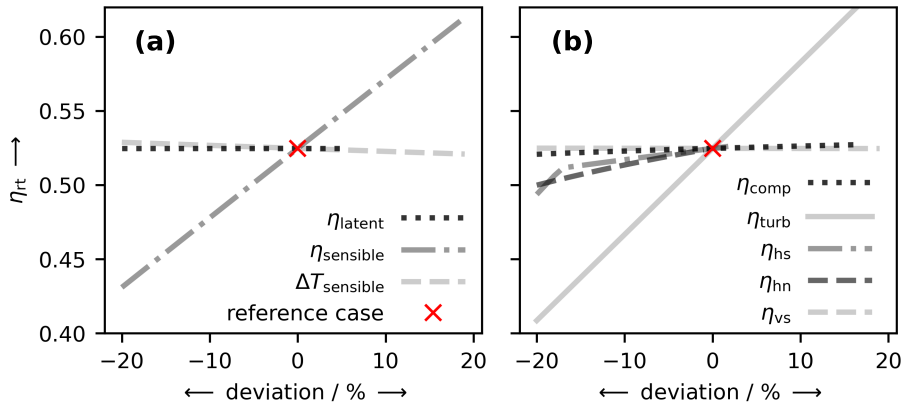

Figure 5. Sensitivity of the RTE to (**a**) heat storage and (**b**) other parameters with respect to a deviation from the reference case. The reference case (red cross) corresponds to the parameters of Table 1.

The parameters are varied by reducing/increasing them by fractions in the range of −20 % to 20 % with respect to the reference case values of Table 1 (indicated by a red cross). Note that to avoid unphysical values, some parameters do not extend over the full x-axis range. For example, all efficiency parameter lines were plotted only up to an efficiency of 100 %. From Figure 5a it becomes apparent that an efficient sensible heat storage system is crucial for the attainment of high RTE. As this holds in general for any storage system which includes the compression and expansion of gases, this observation is to be expected. Conversely, as can be seen from the influence of $\Delta T_{\text{sensible}}$, the heat transfer in the sensible storage unit is of only minor importance. Similarly, η_{latent}, the efficiency of latent heat storage, exhibits hardly any effect on the RTE. That is because in the simulations, ambient heat (at $T_{\text{env}} \gg T_{\text{diss}}$) is used to provide the missing heat of dissociation.

Regarding the performance parameters in Figure 5b, special attention has to be paid to the insentropic turbine efficiency η_{turb}. Its reduction impairs the RTE significantly. Not as dramatic as the effect of η_{turb}, but still important for an efficient plant operation, are the parameters η_{hn} and η_{hs}. These imply the importance of the degree of SP as well as of the air capacity of the SA structure. Remarkably, the slope of η_{hs} changes distinctly at around −17 %. Naturally, a decrease in η_{hs} results in a decrease in RTE, because the mass flow through the turbine decreases. At the same time, though, the sensible heat storage can heat the air to a higher temperature resulting in a higher $W^{\text{a}}_{\text{turb}}$. Yet, beyond a certain point (at around −17 % in Figure 5b), the temperature of the air cannot be increased any further (even though the required amount of heat would be available) because at this point, the minimum temperature difference $\Delta T_{\text{sensible}}$ becomes the limiting factor. As the effect of η_{vs} is negligible, the additional work because of the void space in and between the SA pellets is of no particular interest. The influence of η_{comp}, though minor, is more interesting because its variation affects the RTE in two opposite directions. On the one hand, with a poorer isentropic efficiency, more work is needed for compression. On the other hand, a poorer efficiency also leads to more heat being released. This additional heat can be used to heat the air to higher temperatures before expansion, which in turn results in a larger turbine work. Ultimately, this can almost compensate the additional work needed for compression. Yet, from a technical point of view, it is to be doubted if this additional heat can be fully utilized. Hence, in a more realistic scenario, the influence of η_{comp} on the RTE will most likely be larger than here.

5. Conclusions

Aiming for the development of a novel CES system which overcomes the drawbacks of low RTE and extremely low temperatures in LAES, the most popular CES system to date, a concept for EES in SA, i.e., the clathrate hydrate of air, has been developed and thermodynamically analyzed. Here, the SA acts as a water-based molecular storage vessel for compressed air, which, when released upon dissociation of the SA, drives a gas turbine.

Similar to LAES plants and due to the large heat of SA formation/dissociation and the heat generated during compression, the storage and recovery of heat is crucial for an efficient operation of an SAES plant. Assuming high rates of heat recovery but no utilization of waste heat from external processes, an RTE of 52% is calculated. While this reference case value is already comparable to the maximum RTE envisaged for mature large-scale LAES plants [13], the achievable energy density (47 kWh per m^3 of solidified air) is only half of that of the LAES plants. This is mainly due to a more than three-fold density of air in the liquid, when compared to that in SA.

Nevertheless, as the only components of SA are water and air, the concept of SAES is very friendly to the environment. Moreover, as practically all water can be recycled, water usage is negligible. Additionally, SAES offers some advantages which have the potential to become decisive in a comparison between SAES and LAES. Due to the possible reuse of the water, the addition of thermodynamic promoters is harmless but allows for the careful design of operating conditions. This means that conditions can be adapted to the environmental conditions at the site of the plant or to the conditions needed for the integration of SAES in a larger process. Both options are likely to enable the achievement of significantly higher RTE. Moreover, under the assumption of a pronounced degree of SP, the SA can be readily stored in huge heaps or skips. Therefore, storage tanks are unnecessary and capital expenditures can be reduced.

Though the concept for SAES is well substantiated, for now, the whole concept is purely theoretical. Before proofing the concept in a pilot plant, several questions have to be answered. With respect to the fundamentals, the phenomenon of SP in air hydrates has to be investigated and thoroughly ascertained. The practical goal is to find a route of SA processing which results in the most effective inhibition of SA dissociation at the conditions of storage. Similarly, fast routes for SA formation and dissociation have to be established for typical conditions in an SAES plant. With respect to process engineering, methods for the efficient transport, compression, and expansion of SA have to be studied. These analyses must include the options of processing in a slurry, in pellets, or in dry water hydrate. To better represent a real SAES plant, future models will also need to include multistage compression and expansion of the air, as well as more detailed heat transfer analyses.

In summary, SAES has the potential to compete with its closest competitor LAES, at least in terms of RTEs. This follows from our thermodynamic analysis and potentially milder storage conditions in the case of SAES, of course, given a pronounced degree of SP can be established for hydrates of air. The option to optimize RTEs by adjusting process parameters to the conditions at the plant's site further adds to the appeal of the concept. One particularly interesting option is the idea of combining subsea SAES with offshore wind power generation. There, water and air are abundant. Additionally, hydrostatic pressure aids in compression and allows for storage at thermodynamically stable conditions. Moreover, SA can be readily stored at the seafloor because the buoyancy of SA in water is close to zero.

However, since at the moment the concept is purely theoretical, technical difficulties associated with the processing and storage of SA are hard to foresee. Even if the assumption of a pronounced degree of SP holds, it will be technically very challenging to implement SAES on a large scale. In terms of economics, it will be similarly challenging to even compete with LAES, which has yet to prove itself. Nevertheless, as engineering developments favoring LAES will likely also favor SAES, it seems to early to ultimately decide on the future of SAES. To enable the decision-making on solid grounds, at least the most pressing

open question, namely, that regarding the existence of a pronounced degree of SP in air hydrate, must be clarified first.

Author Contributions: Conceptualization, C.H., B.H. and S.A.; methodology, C.H., B.H., S.H. and S.A.; software, S.H. and S.A.; validation, S.H., B.H. and S.A.; formal analysis, S.H. and S.A.; investigation, S.A.; resources, S.A.; data curation, S.H.; writing—original draft preparation, S.H. and S.A.; writing—review and editing, S.H., B.H. and S.A.; visualization, S.H. and S.A.; supervision, S.A.; project administration, S.A. All authors have read and agreed to the published version of the manuscript.

Funding: The funding from the illwerke vkw Endowed Professorship for Energy Efficiency as well as the Open Access Funding by the Vorarlberg University of Applied Sciences are greatly acknowledged.

Institutional Review Board Statement: Not applicable.

Informed Consent Statement: Not applicable.

Conflicts of Interest: The authors declare no conflict of interest.

Abbreviations

The following abbreviations are used in this manuscript:

CAES	Compressed-air energy storage
CES	Cryogenic energy storage
CP	Cyclopentane
EES	Electrical energy storage
LAES	Liquid-air energy storage
PSH	Pumped-storage hydroelectricity
RTE	Round-trip efficiency
SA	Solidified air
SAES	Solidified-air energy storage
SNG	Solidified natural gas
SP	Self-preservation
STP	Standard temperature and pressure
TBAB	Tetrabutylammonium bromide
THF	Tetrahydrofuran

References

1. Zerrahn, A.; Schill, W.P. Long-run power storage requirements for high shares of renewables: Review and a new model. *Renew. Sustain. Energy Rev.* **2017**, *79*, 1518–1534. [CrossRef]
2. Sterner, M.; Stadler, I. (Eds.) *Handbook of Energy Storage: Demand, Technologies, Integration*; Springer: Berlin/Heidelberg, Germany, 2019. [CrossRef]
3. Child, M.; Kemfert, C.; Bogdanov, D.; Breyer, C. Flexible electricity generation, grid exchange and storage for the transition to a 100% renewable energy system in Europe. *Renew. Energy* **2019**, *139*, 80–101. [CrossRef]
4. Schill, W.P.; Zerrahn, A. Long-run power storage requirements for high shares of renewables: Results and sensitivities. *Renew. Sustain. Energy Rev.* **2018**, *83*, 156–171. [CrossRef]
5. Chen, H.; Cong, T.N.; Yang, W.; Tan, C.; Li, Y.; Ding, Y. Progress in Electrical Energy Storage System: A Critical Review. *Prog. Nat. Sci.* **2009**, *19*, 291–312. [CrossRef]
6. Gür, T.M. Review of Electrical Energy Storage Technologies, Materials and Systems: Challenges and Prospects for Large-Scale Grid Storage. *Energy Environ. Sci.* **2018**, *11*, 2696–2767. [CrossRef]
7. Hameer, S.; van Niekerk, J.L. A Review of Large-Scale Electrical Energy Storage. *Int. J. Energy Res.* **2015**, *39*, 1179–1195. [CrossRef]
8. Rehman, S.; Al-Hadhrami, L.M.; Alam, M.M. Pumped Hydro Energy Storage System: A Technological Review. *Renew. Sustain. Energy Rev.* **2015**, *44*, 586–598. [CrossRef]
9. Kucukali, S. Finding the Most Suitable Existing Hydropower Reservoirs for the Development of Pumped-Storage Schemes: An Integrated Approach. *Renew. Sustain. Energy Rev.* **2014**, *37*, 502–508. [CrossRef]
10. Lu, B.; Stocks, M.; Blakers, A.; Anderson, K. Geographic Information System Algorithms to Locate Prospective Sites for Pumped Hydro Energy Storage. *Appl. Energy* **2018**, *222*, 300–312. [CrossRef]
11. Budt, M.; Wolf, D.; Span, R.; Yan, J. A Review on Compressed Air Energy Storage: Basic Principles, Past Milestones and Recent Developments. *Appl. Energy* **2016**, *170*, 250–268. [CrossRef]

12. Chen, L.; Zheng, T.; Mei, S.; Xue, X.; Liu, B.; Lu, Q. Review and Prospect of Compressed Air Energy Storage System. *J. Mod. Power Syst. Clean Energy* **2016**, *4*, 529–541. [CrossRef]
13. Morgan, R.; Nelmes, S.; Gibson, E.; Brett, G. Liquid Air Energy Storage–Analysis and First Results from a Pilot Scale Demonstration Plant. *Appl. Energy* **2015**, *137*, 845–853. [CrossRef]
14. Ameel, B.; T'Joen, C.; De Kerpel, K.; De Jaeger, P.; Huisseune, H.; Van Belleghem, M.; De Paepe, M. Thermodynamic Analysis of Energy Storage with a Liquid Air Rankine Cycle. *Appl. Therm. Eng.* **2013**, *52*, 130–140. [CrossRef]
15. Guizzi, G.L.; Manno, M.; Tolomei, L.I.; Vitali, R.I. Thermodynamic Analysis of a Liquid Air Energy Storage System. *Energy* **2015**, *93*, 1639–1647. [CrossRef]
16. Sciacovelli, A.; Vecchi, A.; Ding, Y. Liquid Air Energy Storage (LAES) with Packed Bed Cold Thermal Storage – From Component to System Level Performance through Dynamic Modelling. *Appl. Energy* **2017**, *190*, 84–98. [CrossRef]
17. Borri, E.; Tafone, A.; Romagnoli, A.; Comodi, G. A Review on Liquid Air Energy Storage: History, State of the Art and Recent Developments. *Renew. Sustain. Energy Rev.* **2021**, *137*, 110572. [CrossRef]
18. Koh, C.A.; Sloan, E.D.; Sum, A.K.; Wu, D.T. Fundamentals and Applications of Gas Hydrates. *Annu. Rev. Chem. Biomol. Eng.* **2011**, *2*, 237–257. [CrossRef] [PubMed]
19. Miller, S.L. Clathrate Hydrates of Air in Antarctic Ice. *Science* **1969**, *165*, 489–490. [CrossRef]
20. Pauer, F.; Kipfstuhl, S.; Kuhs, W.F.; Shoji, H. Air Clathrate Crystals from the GRIP Deep Ice Core, Greenland: A Number-, Size- and Shape-Distribution Study. *J. Glaciol.* **1999**, *45*, 22–30. [CrossRef]
21. Shoji, H.; Langway, C.C. Air Hydrate Inclusions in Fresh Ice Core. *Nature* **1982**, *298*, 548–550. [CrossRef]
22. Veluswamy, H.P.; Kumar, S.; Kumar, R.; Rangsunvigit, P.; Linga, P. Enhanced Clathrate Hydrate Formation Kinetics at near Ambient Temperatures and Moderate Pressures: Application to Natural Gas Storage. *Fuel* **2016**, *182*, 907–919. [CrossRef]
23. Veluswamy, H.P.; Kumar, A.; Kumar, R.; Linga, P. An Innovative Approach to Enhance Methane Hydrate Formation Kinetics with Leucine for Energy Storage Application. *Appl. Energy* **2017**, *188*, 190–199. [CrossRef]
24. Veluswamy, H.P.; Kumar, A.; Seo, Y.; Lee, J.D.; Linga, P. A Review of Solidified Natural Gas (SNG) Technology for Gas Storage via Clathrate Hydrates. *Appl. Energy* **2018**, *216*, 262–285. [CrossRef]
25. Mohammadi, A.H.; Tohidi, B.; Burgass, R.W. Equilibrium Data and Thermodynamic Modeling of Nitrogen, Oxygen, and Air Clathrate Hydrates. *J. Chem. Eng. Data* **2003**, *48*, 612–616. [CrossRef]
26. Yang, H.; Fan, S.; Lang, X.; Wang, Y.; Sun, X. Hydrate Dissociation Conditions for Mixtures of Air + Tetrahydrofuran, Air + Cyclopentane, and Air + Tetra- *N* -Butyl Ammonium Bromide. *J. Chem. Eng. Data* **2012**, *57*, 1226–1230. [CrossRef]
27. Lipenkov, V.Y.; Istomin, V. On the stability of air clathrate-hydrate crystals in subglacial Lake Vostok, Antarctica. *Mater. Glyatsiol. Issled* **2001**, *91*, 2001.
28. Mohammadi, A.H.; Richon, D. Ice-Clathrate Hydrate-Gas Phase Equilibria for Air, Oxygen, Nitrogen, Carbon Monoxide, Methane, or Ethane + Water System. *Ind. Eng. Chem. Res.* **2010**, *49*, 3976–3979. [CrossRef]
29. Sloan, E.D.; Koh, C.A. *Clathrate Hydrates of Natural Gases*, 3rd ed.; CRC Press: Boca Raton, FL, USA, 2007.
30. Hobbs, P.V. *Ice Physics*; Oxford Classic Texts in the Physical Sciences; Oxford University Press: New York, NY, USA, 2010.
31. Saito, A. Recent Advances in Research on Cold Thermal Energy Storage. *Int. J. Refrig.* **2002**, *25*, 177–189. [CrossRef]
32. Wang, X.; Zhang, F.; Lipiński, W. Carbon Dioxide Hydrates for Cold Thermal Energy Storage: A Review. *Sol. Energy* **2020**, *211*, 11–30. [CrossRef]
33. Yakushev, V.S.; Istomin, V. Gas Hydrates Self-Preservation Effect. In *Physics and Chemistry of Ice*; Maeno, N., Hondoh, T., Eds.; Hokkaido Univ. Press.: Sapporo, Japan, 1992; pp. 136–140.
34. Stern, L.A.; Circone, S.; Kirby, S.H.; Durham, W.B. Anomalous Preservation of Pure Methane Hydrate at 1 Atm. *J. Phys. Chem. B* **2001**, *105*, 1756–1762. [CrossRef]
35. Falenty, A.; Kuhs, W.F.; Glockzin, M.; Rehder, G. 'Self-Preservation' of CH_4 Hydrates for Gas Transport Technology: Pressure–Temperature Dependence and Ice Microstructures. *Energy Fuels* **2014**, *28*, 6275–6283. [CrossRef]
36. Falenty, A.; Kuhs, W.F. 'Self-Preservation' of CO_2 Gas Hydrates—Surface Microstructure and Ice Perfection. *J. Phys. Chem. B* **2009**, *113*, 15975–15988. [CrossRef] [PubMed]
37. Circone, S.; Stern, L.A.; Kirby, S.H.; Durham, W.B.; Chakoumakos, B.C.; Rawn, C.J.; Rondinone, A.J.; Ishii, Y. CO_2 Hydrate: Synthesis, Composition, Structure, Dissociation Behavior, and a Comparison to Structure I CH_4 Hydrate. *J. Phys. Chem. B* **2003**, *107*, 5529–5539. [CrossRef]
38. Takeya, S.; Ripmeester, J.A. Dissociation Behavior of Clathrate Hydrates to Ice and Dependence on Guest Molecules. *Angew. Chem. Int. Ed.* **2008**, *120*, 1296–1299. [CrossRef]
39. Hallbrucker, A.; Mayer, E. Unexpectedly Stable Nitrogen, Oxygen, Carbon Monoxide and Argon Clathrate Hydrates from Vapour-Deposited Amorphous Solid Water: An X-Ray and Two-Step Differential Scanning Calorimetry Study. *J. Chem. Soc. Faraday Trans.* **1990**, *86*, 3785–3792. [CrossRef]
40. Mayer, E.; Hallbrucker, A. Unexpectedly Stable Nitrogen and Oxygen Clathrate Hydrates from Vapour Deposited Amorphous Solid Water. *J. Chem. Soc. Chem. Commun.* **1989**, *12*, 749–751. [CrossRef]
41. Zhang, G.; Rogers, R.E. Ultra-Stability of Gas Hydrates at 1atm and 268.2K. *Chem. Eng. Sci.* **2008**, *63*, 2066–2074. [CrossRef]
42. Rehder, G.; Eckl, R.; Elfgen, M.; Falenty, A.; Hamann, R.; Kähler, N.; Kuhs, W.F.; Osterkamp, H.; Windmeier, C. Methane Hydrate Pellet Transport Using the Self-Preservation Effect: A Techno-Economic Analysis. *Energies* **2012**, *5*, 2499–2523. [CrossRef]

43. Melnikov, V.P.; Podenko, L.S.; Nesterov, A.N.; Drachuk, A.O.; Molokitina, N.S.; Reshetnikov, A.M. Self-Preservation of Methane Hydrates Produced in 'dry Water'. *Dokl. Chem.* **2016**, *466*, 53–56. [CrossRef]
44. Khan, M.N.; Warrier, P.; Peters, C.J.; Koh, C.A. Advancements in Hydrate Phase Equilibria and Modeling of Gas Hydrates Systems. *Fluid Phase Equilibria* **2018**, *463*, 48–61. [CrossRef]
45. Anderson, G.K. Enthalpy of Dissociation and Hydration Number of Carbon Dioxide Hydrate from the Clapeyron Equation. *J. Chem. Thermodyn.* **2003**, *35*, 1171–1183. [CrossRef]
46. Anderson, G.K. Enthalpy of Dissociation and Hydration Number of Methane Hydrate from the Clapeyron Equation. *J. Chem. Thermodyn.* **2004**, *36*, 1119–1127. [CrossRef]
47. Hester, K.C.; Huo, Z.; Ballard, A.L.; Koh, C.A.; Miller, K.T.; Sloan, E.D. Thermal Expansivity for sI and sII Clathrate Hydrates. *J. Phys. Chem. B* **2007**, *111*, 8830–8835. [CrossRef] [PubMed]
48. Kuhs, W.; Chazallon, B.; Radaelli, P.; Pauer, F. Cage Occupancy and Compressibility of Deuterated N_2-Clathrate Hydrate by Neutron Diffraction. *J. Incl. Phenom. Mol. Recognit. Chem.* **1997**, *29*, 65–77. [CrossRef]
49. Takeya, S.; Honda, K.; Yoneyama, A.; Hirai, Y.; Okuyama, i.; Hondoh, T.; Hyodo, K.; Takeda, T. Observation of Low-Temperature Object by Phase-Contrast x-Ray Imaging: Nondestructive Imaging of Air Clathrate Hydrates at 233 K. *Rev. Sci. Instrum.* **2006**, *77*, 053705. [CrossRef]
50. Bell, I.H.; Wronski, J.; Quoilin, S.; Lemort, V. Pure and Pseudo-pure Fluid Thermophysical Property Evaluation and the Open-Source Thermophysical Property Library CoolProp. *Ind. Eng. Chem. Res.* **2014**, *53*, 2498–2508. [CrossRef] [PubMed]